Indonesian Journal of Science & Technology

Journal homepage: http://ejournal.upi.edu/index.php/ijost/

Ganciclovir-Loaded Chitosan Nanoparticles and Their Activity against HSV-1 Inducing Herpetic Retinitis

Lidya Agriningsih Haruna[1], La Ode Muhammad Julian Purnama[1], Adryan Fristiohady[2], Promsin Masrinoul[3], Jukrapun Komaikul[3], Kunjimas Ketsuwan[3], Rathapon Asasutjarit[1,]*

[1]Thammasat University, 12120, Pathum Thani, Thailand
[2]Universitas Halu Oleo, Kendari, Indonesia
[3]Mahidol University, Nakhon Pathom, Thailand
*Correspondence: E-mail: rathapon@tu.ac.th, rathapona@hotmail.com

ABSTRACT

Herpes simplex virus (HSV)-1-induced retinitis is one of ophthalmic viral infections. It is found in some immunocompromised and elderly patients and is a cause of complete blindness. Nowadays, an intravitreal (IVT) injection of ganciclovir (GCV) is applied to treat this disease. Unfortunately, frequent IVT injections induce adverse effects in the eye. GCV-loaded chitosan nanoparticles (GCV-CS-NPs) were developed to reduce the number of IVT injections. This study developed GCV-CS-NPs and investigated their activity against HSV-1. GCV-CS-NPs were prepared using an ionic gelation method with varying formulation compositions. The particle size, polydispersity index (PDI), zeta potential, pH, drug release, and activity against the HSV-1 were investigated. The results showed GCV-CS-NPs with particle sizes of around 161 to 294 nm, moderate PDI values, and zeta potentials of between +8.0 and +18.1 mV. These properties strongly depended on the formulation compositions. The release rate of GCV from the optimized GCV-CS-NPs (3C-0.5G-1T-4.5) in the simulated vitreous humor regarding Higuchi's model was 4.89±0.48 µg/min1/2. The IC50 against the HSV-1 was 25.12±0.02 µg/mL. 3C-0.5G-1T-4.5 could be accepted as a promising delivery system of GCV to the vitreous humor via IVT injection and had a potential for being subjected to further in vivo studies.

ARTICLE INFO

Article History:
Submitted/Received 19 Nov 2024
First Revised 18 Dec 2024
Accepted 27 Feb 2025
First Available Online 28 Feb 2025
Publication Date 01 Apr 2025

Keyword:
Chitosan nanoparticles,
Ganciclovir,
Herpes simplex virus,
Intravitreal injection,
Retina.

1. INTRODUCTION

Herpes Simplex Virus-1 (HSV-1) is a major virus causing herpetic retinitis in immunocompromised and elderly patients. It results in acute retinal necrosis with uveitis, occlusive vasculitis, and retinal detachment. Therefore, HSV-1 is one of the causes of permanent vision loss in these patients [1]. Currently, around 1.3 persons per 10,000,000 population are suffering from herpetic retinitis [2]. Although the prevalence rate of this disease is low, it is a serious sight-threatening eye conditions that cause complete blindness.

Ganciclovir (GCV) is an antiviral agent that is effective in the treatment of ophthalmic viral infections. The mechanism of its action is a competitive inhibitor of the viral deoxyribonucleic acid polymerase. It interferes with a process of viral DNA synthesis that leads to the failure of a virus particle replication process. GCV is classified as a drug in the Biopharmaceutical Classification System (BCS) class III. Its water solubility is 4.3 mg/mL with a logP of -1.66 (25˚C). However, the solubility of GCV could be improved using either a strong acid or a strong base because GCV possesses two pKas, i.e., pKa1 (2.2) and pKa2 (9.4) [3].

Currently, GCV is used for the treatment of viral retinitis via intravitreal injection, which is recognized as an effective method for delivery of GCV in treatment of the herpetic retinitis because it bypasses the drug absorption phase by directly crossing the posterior eye segment barriers and rapidly provides the effective concentration of GCV against the HSV-1 in the vitreous humor [4,5]. However, IVT injection of GCV solution requires more frequencies at the beginning period to reach the effective concentration and to maintain the therapeutic concentration of GCV in the retinal tissue. Unfortunately, the repetition of IVT injection usually induces pain, risks of retinal detachment, and endophthalmitis. It always reduces patient compliance and causes failure in the treatment [6,7].

To date, polymeric nanoparticles (NPs) that are solid particles comprising of biocompatible polymers with a size of 10-1000 nm have been widely used as delivery systems of various drugs via IVT injection, e.g., poly(lactic-co-glycolic) acid [8,9], albumin [9], Pluronic block copolymers F68 and F127 [10], and chitosan (CS) [11]. These polymeric NPs possess the ability to control drug release [12] and protect drug molecules from environment-induced degradation [13]. Therefore, these NPs can control the drug release and prolong the half-life of many drugs in the vitreous humor [14] as reported in previous publications, for example, dexamethasone palmitate (DXP) [10], bevacizumab [9], and melphalan [8].

CS is a natural linear polysaccharide polymer. It consists of acetylation and deacetylation units of D-glucosamine and N-acetylglucosamine linked by 1,4-glycosidic bonds [15]. Due to its biocompatibility and mucoadhesiveness properties, CS has been applied as an ophthalmic drug delivery system for both anterior [16] and posterior eye segments [17].

CS NPs (CS-NPs) are one the polymeric NPs consisting of CS as a polymeric matrix [18]. They can be prepared by an ionotropic gelation technique via ionic interactions between positive and negative charges of CS polymeric chains and a crosslinking agent, e.g. tripolyphosphate (TPP), respectively [19,20]. CS-NPs not only protect the loaded drug from degradation induced by the biological environment but also control the drug release through the polymeric matrix [21]. CS-NPs can prolong the drug half-life in the target tissue, and significantly improve drug bioavailability [22]. Although CS-NPs have been applied as a delivery system of various drugs via IVT injection, e.g., bevacizumab [23,24], dexamethasone [25], ranibizumab [26], there is still lack of data of CS-NPs applications for delivery of GCV via IVT injection to eradicate the HSV-1 inducing retinitis.

DOI: https://doi.org/10.17509/ijost.v10i1.80998
p- ISSN 2528-1410 e- ISSN 2527-8045

This study thus aimed to develop formulations of GCV-CS-NPs, to determine the effect of formulation compositions on their physicochemical properties, and to investigate the *in vitro* antiviral activity of these NPs.

2. METHODS

2.1. Chemicals

Medium chain CS (Mn = 110 kDa, Mw = 620 kDa) with a degree of deacetylation of 74.9%, TPP, 3-(4,5-dimethylthiazol-2-yl)-2,5-diphenyltetrazolium Bromide (MTT) were provided by Sigma-Aldrich Co., Ltd. (St. Louis, MO, USA). Tween 80 was obtained from P. C Drug Center Co. Ltd (Bangkok, Thailand). Hydrochloric acid (HCl) was purchased from QRec Co., Ltd. (Auckland, New Zealand). Ganciclovir (>98% purity) was purchased from TCI Co., Ltd. (Tokyo, Japan). Sodium hydroxide was obtained from Lab-Scan Co., Ltd. (Bangkok, Thailand). Isopropanol, methanol, and acetonitrile (an HPLC grade with 99% purity) were supplied by Fisher Chemical Co., Ltd. (Loughborough, Leicestershire, UK). Potassium dihydrogen phosphate was obtained from Ajax Finechem Co., Ltd. (Auckland, New Zealand).

2.2. Cell Culture

The Arising Retinal Pigment Epithelial cells (ARPE-19 cells; CRL-2302) were purchased from the American Type Culture Collection (ATCC Inc. Manassas, Virginia, USA). Dulbecco's Modified Eagle Medium (DMEM)-F12 was purchased from Cytiva, HyClone™ Inc. (Logan, UT, USA). Fetal bovine serum (FBS), penicillin/streptomycin, phosphate-buffered saline (PBS), and trypsin were purchased from Invitrogen Corp., (Carlsbad, California, USA).

The ARPE-19 cells were cultured in DMEM-F12 complete medium with 10% FBS, and 1% penicillin/streptomycin (1,000 U/mL penicillin and 100 µg/mL streptomycin). The cells were incubated at 37°C under a 5% CO_2 atmosphere.

2.3. Preparation of GCV-CS-NPs

GCV-CS-NPs were prepared using the ionotropic gelation technique as described elsewhere [20]. Briefly, CS was dispersed in an HCl solution (0.1 M) and was stirred continuously until a clear solution was obtained. Meanwhile, GCV and Tween 80 were separately dissolved in an HCl solution (0.01 M) before slowly dropping into the CS solution. The mixture of GCV in the CS solution was continuously stirred using a high-speed stirrer (Ultra-Turrax T8, Germany). Then, a TPP solution in distilled water was added to the mixture under vigorous stirring by the high-speed stirrer for 1 h. The formulations of GCV-CS-NPs prepared in this study varied in the weight ratios of CS/GCV/TPP as shown in **Table 1**.

The obtained GCV-CS-NPs were separated from the vehicles using the ultrafiltration technique according to the following details. GCV-CS-NPs in the vehicle were loaded into a stirred ultrafiltration cell (Millipore, USA) with a polyvinylidene fluoride filtration disc (10 kDa MWCO). Nitrogen gas was applied to the cell at a pressure of 2 PSI until the vehicle was completely removed from GCV-CS-NPs. Thereafter, the obtained GCV-CS-NPs were reconstituted with PBS (pH 7.4) and used for further experiments.

To investigate the effect of pH values on the physicochemical properties of GCV-CS-NPs, the pH of the vehicle, which was called later a "production medium", was adjusted to 2.0, 4.5, and 5.5 using a sodium hydroxide solution (0.1 N) before the addition of a TPP solution into the solution of CS and GCV. Then, the obtained mixture was continuously stirred with the high-speed stirrer for 1 h before removing the production medium from the GCV-CS-NPs and reconstituting it with PBS (pH 7.4).

DOI: https://doi.org/10.17509/ijost.v10i1.80998
p- ISSN 2528-1410 e- ISSN 2527-8045

2.4. Characterization of GCV-CS-NPs

2.4.1. Measurement of particle size, polydispersity index, zeta potential, and pH

Particle size, Polydispersity Index (PDI), and zeta potential of GCV-CS-NPs were analyzed by a dynamic light scattering technique and an electrophoretic light scattering, respectively, via a Zetasizer (Malvern Instrument NanoZS, UK). The pH value of the samples was measured by a pH meter (Mettler-Toledo, SevenCompact™ pH/ Ionmeters S220, Switzerland). The measurements were performed in triplicate.

2.4.2. Determination of drug entrapment efficiency

The drug entrapment efficiency (EE) of GCV-CS-NPs was determined using the stirred ultrafiltration cell with the same condition as previously described. The filtrate obtained from the ultrafiltration process was analyzed for free GCV content using a UV-visible spectrophotometer (Shimadzu UV-Vis UV-1800, Japan) at a wavelength of 254 nm [27]. *EE (%)* of the NPs was calculated using equation (1).

$$\text{EE (\%)} = \frac{(\text{Total Amount of Drug Loaded} - \text{Drug Content})}{\text{Total Amount of Drug Loaded}} \text{x}100 \quad (1)$$

2.4.3. Morphological observation of GCV-CS-NPs using Scanning Electron Microscope Technique (SEM) and Transmission Electron Microscope Technique (TEM)

The morphology of the optimized GCV-CS-NPs was observed by both a scanning electron microscopy (SEM) and transmission electron microscopy (TEM) technique. The protocols of sample preparation for each technique were described in the following details.

Regarding the SEM technique, the sample was dropped to copper stubs and dried under ambient conditions. The sample surface was coated with gold. The micrographs were taken using a FESEM-EDS (JEOL JSM-IT800SHL, Japan) at 2 kV [28,29].

For the TEM investigation, the internal morphology of the optimized GCV-CS-NPs was observed using transmission electron microscopy (TEM). One drop of each sample was placed on a copper grid coated with carbon films. Then, it was stained with 2% w/v phosphotungstic acid solution, and dried at room temperature. The images were captured using a Transmission electron microscope (JEM-2100, JEOL Inc., Tokyo, Japan) at 200 kV [27].

2.4.4. Attenuated total reflectance-fourier transform infrared spectroscopy analysis of GCV-CS-NPs

To determine interactions between GCV and the ingredients of CS-NPs, an Attenuated Total Reflectance-Fourier transform infrared spectroscopy (ATR-FTIR) technique was performed. In this study, the samples (50 µL) were directly transferred and dropped on a crystal surface. Then, the ATR-FTIR spectra of CS, GCV, and GCV-CS-NPs were provided using an ATR-FTIR diamond spectrometer (Nicolet iS5, Thermo Fisher Scientific, USA) at wavenumbers from 400-4000 cm^{-1} [28].

2.5. Release Studies of GCV from GCV-CS-NPs

2.5.1. Release study of GCV from GCV-CS-NPs in PBS (pH 7.4)

Release kinetics of GCV from the optimized GCV-CS-NPs were determined using Franz diffusion cells. One mL of a representative GCV-CS-NPs suspension, which was reconstituted with PBS (pH 7.4) to obtain 0.1 % w/v of GCV after GCV-CS-NPs were separated from the production medium, was loaded into a donor compartment of the cells. The receptor unit was filled with PBS (pH 7.4) and maintained at 37±1 °C. A cellulose dialysis membrane (Sigma-

DOI: https://doi.org/10.17509/ijost.v10i1.80998
p- ISSN 2528-1410 e- ISSN 2527-8045

Aldrich, USA) with a molecular weight cut-off (MWCO) of 12 kDa was placed between the donor and receptor unit. Five mL of the receiving medium was withdrawn from the receptor unit at 5, 10, 15, 30, 60, 120, 180, 240, 300, 360, 420, and 480 min. It was replenished with an equal volume of fresh PBS (pH 7.4). The withdrawn samples were analyzed for the GCV content using a UV spectrophotometer at a wavelength of 254 nm in triplicate.

The data from this study were then analyzed for the most appropriate kinetic model based on a determination coefficient (r^2) that represented a goodness of fit for the selected kinetic model [30].

2.5.2. Diffusion study of GCV through a simulated vitreous humor

Diffusion study of GCV from GCV solution and the optimized GCV-CS-NPs through the simulated vitreous humor (SVH) were investigated using Franz diffusion cells with the same protocol as used in the determination of drug release GCV-CS-NPs. The condition of this study imitated the diffusion of GCV from the dosage forms through the vitreous humor before reaching the retinal tissue [31]. Briefly, one mL of each sample containing 0.1 % w/v of GCV was dispersed into the SVH at a weight ratio of 1:10, respectively, and mixed thoroughly. The samples were loaded into the donor compartment of the diffusion cells which was assembled with a receptor unit containing PBS (pH 7.4) and maintained at 37±1 °C. A cellulose dialysis membrane (Sigma-Aldrich, USA) with 12 kDa MWCO, was placed between the donor and receptor unit. Five mL of the receiving medium was withdrawn from the receptor chamber at 5, 10, 15, 30, 60, 120, 180, 240, 300, 360, 420, and 480 min with replenishment of an equal volume of fresh PBS (pH 7.4). The withdrawn receiving media were analyzed for the GCV content using a UV spectrophotometer at a wavelength of 254 nm in triplicate.

The SVH used in this study contained agar powder (MW 336.34 g/mol) (bacteriological grade, GRM026P, Himedia, India) and hyaluronic acid (MW 1000 kDa) (H7630, Sigma-Aldrich Co., Ltd, St. Louis, MO, USA) at a concentration of 0.2 %w/v and 0.5 %w/v, respectively, in PBS (pH 7.4) [32].

2.6. An *in vitro* Cytotoxicity Test by MTT Assay

The MTT assay was performed to determine the cytotoxicity of GCV solution (0.1% w/v) and GCV-CS-NPs containing GCV 0.1% w/v to the ARPE-19 cells.

The cells were seeded in 96-well plates with a density of $0.1x10^5$ cells/well/100 µl. After reaching confluence, they were treated for 24 h with various concentrations of GCV solution, optimized GCV-CS-NPs, and Blank-CS-NPs, which were CS-NPs containing the same compositions as the optimized GCV-CS-NPs without the addition of GCV. The test samples were diluted with the complete medium to obtain various concentrations of GCV as follows: 0.05, 0.1, 0.5, 1, 5, 10, 50, and 100 µg/mL. These concentrations were called later "equivalent concentrations". For Blank-CS-NPs, their equivalent concentration was calculated based on the concentration of GCV-CS-NPs that provided the required equivalent concentrations.

After the incubation period, the test samples were removed from the wells. The cells were washed twice with PBS (pH 7.4) and replaced with a fresh complete medium (100 µL). The MTT solution in PBS pH 7.4 (0.5 mg/ml) was added into the wells and incubated for 4 h. Formazan crystals in the cells were extracted using 0.04 N HCl-isopropanol after the MTT solution was removed from the plates, and then incubated for 60 min in the dark at a room temperature. The optical density (OD) of each well was measured by a microplate reader (Spectrostar Omega BMG Labtech, Ortenberg, Germany) at a wavelength of 570 nm. The experiment was performed in triplicate. The cell viability (CV) of the ARPE-19 cells was calculated following equation (2).

DOI: https://doi.org/10.17509/ijost.v10i1.80998
p- ISSN 2528-1410 e- ISSN 2527-8045

$$CV\ (\%) = (OD_{sample} / OD_{control}) \times 100 \quad (2)$$

where OD_{sample} and $OD_{control}$ were the OD of wells containing the cells that were incubated with the test samples, and that of the wells containing the cells without any treatments, respectively. The test samples were considered to be cytotoxic to the cells if the CV (%) was less than 70% [23].

2.7. Determination of Activity of GCV-CS-NPs Against HSV-1

2.7.1. Cell culture and virus preparation

An anti-HSV-1 activity of the test samples, i.e., GCV solution, optimized GCV-CS-NPs, and Blank-CS-NPs, was determined by a plaque reduction assay as described in the previous publications with some modifications [33,34]. Briefly, the ARPE-19 cells were seeded into 96-well plates at a density of $1x10^4$ cells/well/100 µl. They were incubated until they were confluent. Then, the culture medium was removed and replaced with a suspension of HSV-1 (KOS strain, VR-1493; ATCC, USA) at a multiplicity of infection (moi) of $1x10^{-3}$ per well. The ARPE-19 cells were incubated with the HSV-1 for 1h before being washed to eliminate the free HSV-1 in the medium with PBS (pH 7.4). After that, the infected ARPE-19 cells were incubated with the test samples at various equivalent concentrations for 24 h.

When the incubation was complete, the supernatant was removed from each well. The cells were washed again with PBS (pH 7.4) and further incubated in a fresh complete medium for 48 h. The medium in each well was later collected to determine the virus titer by the plaque assay in the other ARPE-19 cells.

2.7.2. Plaque assay

The ARPE-19 cells were seeded in 96-well plates at a density of $1x10^4$ cells/well. After the confluence, these cells were washed with PBS (pH 7.4) and incubated with the medium that was collected from the infected ARPE-19 cells, for 24 h. The media were later discarded and replaced with one hundred µl of carboxymethylcellulose solution (0.8% w/v in the complete medium) to overlay the cell layer in each well. The overlaid ARPE-19 cells were incubated for 48 h. Thereafter, the carboxymethylcellulose solution in each well was removed. The cells were washed with PBS (pH 7.4) and fixed with 4% v/v of formaldehyde/PBS.

The virus plaques in the ARPE-19 cell layers were stained with anti-HSV-1 ICP4, the infected cell protein antibodies 10F1, (Cat. No. Ab6514, Abcam, Trumpington, Cambridge, UK). The cytopathic effect (CPE) of the cells was observed under a converted light microscope (Nikon ECLIPSE Ts2R, Nikon Corporation, Tokyo, Japan). The plaque numbers were counted and reported as plaque-forming units/mL (pfu/mL). The half-maximal inhibitory concentration (IC_{50}) of the test samples was determined using GraphPad Prism 5.0 [33,34].

2.8. Statistical Analysis

The obtained results were presented as a mean ± SD. The data were statistically analyzed using a one-way ANOVA with Tukey's post-hoc test at a significant level of 0.05 via SPSS Statistic Software, Version 22 (IBM, USA).

3. RESULTS AND DISCUSSION

3.1. Preparation of GCV-CS-NPs

GCV-CS-NPs containing various weight ratios of CS/GCV/TPP were prepared using the ionotropic gelation technique. Their particle size, PDI, and zeta potential were measured and shown in **Table 1**. The obtained GCV-CS-NPs had particle size in a range of 161-294 nm with

DOI: https://doi.org/10.17509/ijost.v10i1.80998
p- ISSN 2528-1410 e- ISSN 2527-8045

moderate to high PDI of around 0.4-0.7. Their zeta potentials were in a range of positive values of 8.0 to 18.1 mV depending on the compositions of the GCV-CS-NPs.

Regarding the mean monomeric molecular weight of CS of 169 g/mol [35], the molecular weight of GCV, and TPP, which are, 255 g/mol [36], and 368 g/mol [29], respectively, the mole ratio of CS/(GCV+TPP) of all GCV-CS-NPs were more than 1.00 as reported in **Table 1**. The content of a positively charged CS was more than the total content of GCV and TPP that contained negative charges in their molecules.

Since GCV-CS-NPs were formed by the ionic interactions between the cationic ions in CS and the anionic ions in GCV and TPP molecules, GCV-CS-NPs thus exhibited the net charges from the neutralization of the counter ions on their surfaces. Generally, CS contains one positive charge per deacetylated monomer. In this particular case, CS had around 0.8 positive charges per monomer regarding its deacetylation degree of 74.9% [37]. Meanwhile, GCV and TPP consecutively have two and five negative charges per mole at the preparation condition (pH 2.0). Therefore, the positive/negative charge ratios of cations to anions consisting of GCV-CS-NPs were lower than 1.00 as shown in **Table 1**. All GCV-CS-NPs should have net negative charges. However, **Table 1** shows that the obtained GCV-CS-NPs had positive zeta potential values. The anions in the GCV-CS-NPs were unable to completely interact with the positive charges in CS. These findings could be explained by the charge spacing in anion moieties and steric impediments in the polymeric chains of CS. They limited the neutralizations of these counter ions. Finally, the positive charges were remained and expressed on the surface of GCV-CS-CPs [38].

The %EE of GCV-CS-NPs shown in **Table 1** indicated the relatively low GCV contents that were entrapped in all NPs, around 6.5% to 23.8%. These results were from the incomplete ionization of GCV at the pH of 2.0, which was a condition of production, whereas one of the pKa of GCV is 2.2 [39]. In the production process, GCV was dissolved in the HCl solution (pH 2.0). The hydroxyl groups in GCV were partially deprotonated and provided some negative charges in GCV molecules. The ionic interactions between the amino groups of CS and the negatively charged moieties in GCV also partially occurred.

3.1.2. Effect of CS content on particle size, PDI, and zeta potential of GCV-CS-NPs

To investigate the effect of CS content on particle size, PDI, and zeta potential of GCV-CS-NPs, these particular parameters of 2C-1G-1T, 3C-1G-1T, and 4C-1G-1T were compared. The results shown in **Table 1** indicated that an increase in CS content significantly affected the particle size of GCV-CS-NPs at a fixed content of GCV and TPP in 2C-1G-1T, 3C-1G-1T, and 4C-1G-1T, at a *p*-value of 0.000. This is because the more content of CS, the more interactions between polymeric chains. For example, the hydrogen bonds, hydrophobic attractions, and electrostatic repulsions between the cationic amino groups in CS [40]. They limit the approach of each polymeric chain before crosslinking with the anions of GCV and TPP, the larger particle size of GCV-CS-NPs was thus formed [41].

The effect of CS on PDI was found when the ratio of CS/GCV/TPP was increased from 2:1:1 to 4:1:1. The 4C-1G-1T contained the highest content of CS had the significantly highest value of PDI as seen in **Table 1**. Its PDI was higher than that of 3C-1G-1T, and 2C-1G-1T at a *p*-value of 0.001 and 0.001, respectively. The higher CS content resulted in the higher viscosity of the CS solution. A constant force from the homogenizer that was provided to the mixed solution of the ingredients of GCV-CS-NPs during the homogenization process was not sufficient to generate a homogeneous particle size of GCV-CS-NPs. It thus led to a broader particle size distribution represented as a large PDI value of GCV-CS-NPs [41,29].

DOI: https://doi.org/10.17509/ijost.v10i1.80998
p- ISSN 2528-1410 e- ISSN 2527-8045

Table 1. Physicochemical characterization of GCV-CS-NPs prepared at a pH of 2.0, (mean ± SD; n=3).

Formulation	A weight ratio of CS/GCV/TPP	Particle Size (nm)	PDI	Zeta potential (mV)	The mole ratio of CS/ (GCV +TPP)	+/- charge ratio	%EE
2C-1G-1T	2: 1:1	191±6	0.6±0.0	+8.0±0.4	1.8	0.4	6.5±0.6
3C-1G-1T	3:1:1	228±10	0.6±0.0	+10.9±0.8	2.7	0.7	10.9±0.4
4C-1G-1T	4:1:1	294±6	0.7±0.0	+15.7±1.2	3.6	0.9	15.4±0.2
3C-0.5G-1T	3:0.5:1	166±3	0.4±0.1	+17.5±0.2	3.8	0.8	19.6±1.3
3C-0.25G-1T	3:0.25:1	161±6	0.4±0.0	+18.1±1.5	4.8	0.9	23.8±0.1

The results in **Table 1** additionally suggested that the higher CS contents in GCV-CS-NPs formulations caused the higher zeta potential of GCV-CS-NPs. This phenomenon could be noticed in the case of 4C-1G-1T, 3C-1G-1T, and 2C-1G-1T. 4C-1G-1T exhibited the highest zeta potential value when compared to that of 3C-1G-1T (a *p*-value = 0.016) and 2C-1G-1T (a *p*-value = 0.000), respectively. This is due to the greater availability of positively charged-amine groups in CS that remained after the neutralization with a fixed negatively charged-GCV and TPP content in the formulations. They were thus expressed positive values of the zeta potential on the surface of GCV-CS-NPs. Furthermore, an increase in CS contents significantly improved the %EE of GCV in GCV-CS-NPs (a *p*-value = 0.000). The results were due to the more electrostatic interactions between CS and GCV, which facilitated better encapsulation of the drug within GCV-CS-NPs.

Since 3C-1G-1T had the optimum particle size, PDI zeta potential, and %EE, it was selected as a representative for further development.

3.1.3. Effect of GCV content on particle size, PDI, and zeta potential of GCV-CS-NPs

In this study, the effect of GCV content on the particle size of GCV-CS-NPs was investigated based on the 3C-1G-1T which was chosen from the previous section. Therefore, the formulation of 3C-0.5G-1T and 3C-0.25G-1T were included in the development.

When the GCV content was increased, the larger particle size of GCV-CS-NPs was obtained (**Table 1**). Regarding 3C-1G-1T, it contained the highest content of GCV, and it had a larger particle size than 3C-0.5G-1T and 3C-0.25G-1T at a *p*-value = 0.000 and 0.000, respectively. The higher GCV content in the formulation led to more interactions between GCV and CS polymeric chains via electrostatic interactions [42-44]. More GCV molecules were thus entrapped in the nanoparticle matrix causing larger particle size. This obtained result aligned with other researchers [45]. They found that more drug content in rivastigmine-loaded L-lactide-depsipeptide NPs resulted in larger particle sizes.

The obtained results also pointed out that the PDI of 3C-1G-1T was higher than that of 3C-0.5G-1T and 3C-0.25G-1T (*p*-value = 0.004 and 0.000, respectively) with significantly lower zeta potential than that of 3C-0.5G-1T and 3C-0.25G-1T (*p*-value = 0.007 and 0.002, respectively). These findings were the results of the higher GCV content in 3C-1G-1T, it caused more neutralization with the cations in CS and led to lower positive charges on the surface of GCV-CS-NPs. The repulsion forces between GCV-CS-NPs were weakened. Therefore, 3C-1G-1T tended to aggregate and became larger in particle size with a broader distribution. It thus completely precipitated within 24 hours after preparation.

According to the result shown in **Table 1**, the %EE of 3C-1G-1T was lower than that of 3C-0.5G-1T (*p*-value = 0.000) and 3C-0.25G-1T (*p*-value = 0.000). Although the highest content of

DOI: https://doi.org/10.17509/ijost.v10i1.80998
p- ISSN 2528-1410 e- ISSN 2527-8045

GCV was loaded into the formulation, only around 11% of the total drug was entrapped in 3C-1G-1T. Moreover, when the weight of entrapped GCV was considered, the GCV content in 3C-1G-1T (0.11 mg) was comparable to that of 3C-0.5G-1T (0.10 mg) and was higher than that of 3C-0.25G-1T (0.06 g). This finding indicated the effect of rigid charge spacings in the anion moieties of GCV and steric hindrances in the CS structure. They retarded the interactions between GCV and CS and limited the %EE of GCV in 3C-1G-1T. Since 3C-0.5G-1T could entrap a high content of GCV with optimum particle size, PDI, and zeta potential, it was selected as a representative for the next studies.

3.3.4. Effect of pH on particle size, PDI, zeta potential, and %EE of 3C-0.5G-1T

Since the pKa (pKa1) of GCV and CS is 2.2 [39] and 6.5 [46], respectively, the pH for GCV-CS-NPs preparation is a crucial factor affecting the solubility of GCV and CS. In addition, since GCV-CS-NPs prepared in this study aimed for delivery of GCV into the eye via the IVT injection, the pH of the obtained GCV-CS-NPs should be compatible with the eye tissue. Generally, the ideal pH of the intravitreal products is around 7.4, which is the pH of the vitreous humor [47,48]. However, this pH rapidly led to the precipitation of both GCV and CS during the production process. Therefore, the determination of an optimum pH for the preparation of GCV-CS-NPs was performed by varying the pH of the production medium at a pH of 4.5 and 5.5. Regarding the most acceptable characteristics of 3C-0.5G-1T, it was chosen as a representative and was included in this study as GCV-CS-NPs that were prepared at a pH of 2.0.

Table 2 demonstrates that when the pH of the production medium was increased, particle size, PDI, zeta potential, and *%EE* of 3C-0.5G-1T were significantly changed. The results indicated that the higher the pH, the higher the particle size (*p*-value = 0.000) and PDI (*p*-value = 0.000) [49,50]. On the contrary, the higher pH induced the lower zeta potential of GCV-CS-NPs. These behaviors were from the reduction of protonation of CS the higher pHs [49,51,52]. It weakened electrostatic repulsions between the polymeric chains and led to the aggregation of GCV-CS-NPs. However, at the pH of 4.5 and 5.5, GCV was still completely dissolved in the production medium, but it needed a longer time to accomplish. The reduced protonation of CS lowered %EE because it decreased the degree of electrostatic interactions between the positive charges of CS and the negative charges of GCV. Therefore, the %EE of 3C-0.5G-1T-5.5 was less than that of 3C-0.5G-1T and 3C-0.5G-1T-4.5 at a *p*-value of 0.000 and 0.000, respectively.

Since 3C-0.5G-1T-4.5 possessed the optimum particle size, PDI with the moderate zeta potential, and highest %EE when compared to that of 3C-0.5G-1T and 3C-0.5G-1T-5.5 (*p*-value = 0.000, and 0.000, respectively), it was chosen for the next experiments.

Table 2. Physicochemical characterization of 3C-0.5G-1T at various pHs, (mean ± SD; n=3).

pH	Formulation	Particle Size (nm)	PDI	Zeta potential (mV)	%EE
2.0	3C-0.5G-1T	166±3	0.4±0.1	+17.5±0.2	19.6±1.3
4.5	3C-0.5G-1T-4.5	173±7	0.4±0.0	+14.8±1.1	28.5±0.5
5.5	3C-0.5G-1T-5.5	190±5	0.5±0.1	+11.3±1.0	3.8±2.3

3.2 Morphology observation of 3C-0.5G-1T-4.5

The morphology of 3C-0.5G-1T-4.5 (a representative of GCV-CS-NPs) was observed using the SEM and TEM techniques, as illustrated in **Figure 1**. The SEM micrograph in **Figure 1 (a)** shows that 3C-0.5G-1T-4.5 has a spherical shape with a smooth surface. Their particle size was around 200 nm with a relatively broad size distribution. Meanwhile, the TEM analysis

DOI: https://doi.org/10.17509/ijost.v10i1.80998
p- ISSN 2528-1410 e- ISSN 2527-8045

shown in **Figure 1 (b)** further confirms the nanoscale dimensions, revealing a particle size of approximately 200 nm. Additionally, TEM micrographs suggest a uniform structure with no obvious aggregation, which was from the electrostatic repulsions between the positive charges on the surface of 3C-0.5G-1T-4.5 [53,54].

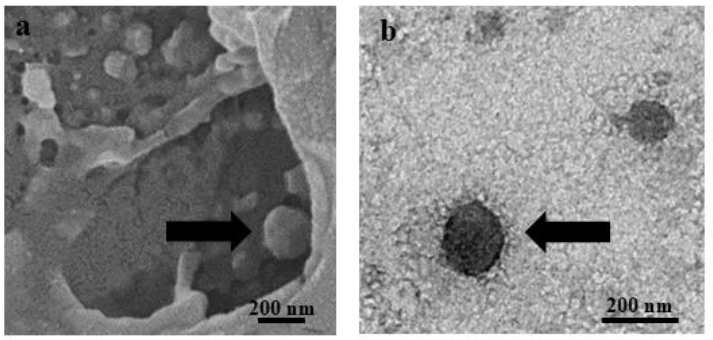

Figure 1. (a) SEM and (b) TEM micrographs of 3C-0.5G-1T-4.5

3.3. FTIR analysis of CS, GCV, and 3C-0.5G-1T-4.5

The FTIR analysis was conducted to identify the interactions between GCV and the compositions of GCV-CS-NPs [55]. In this study, 3C-0.5G-1T-4.5 was selected as a representative of GCV-CS-NPs. Its FTIR spectrum is shown in **Figure 2** with the presentation of the FTIR of CS and GCV.

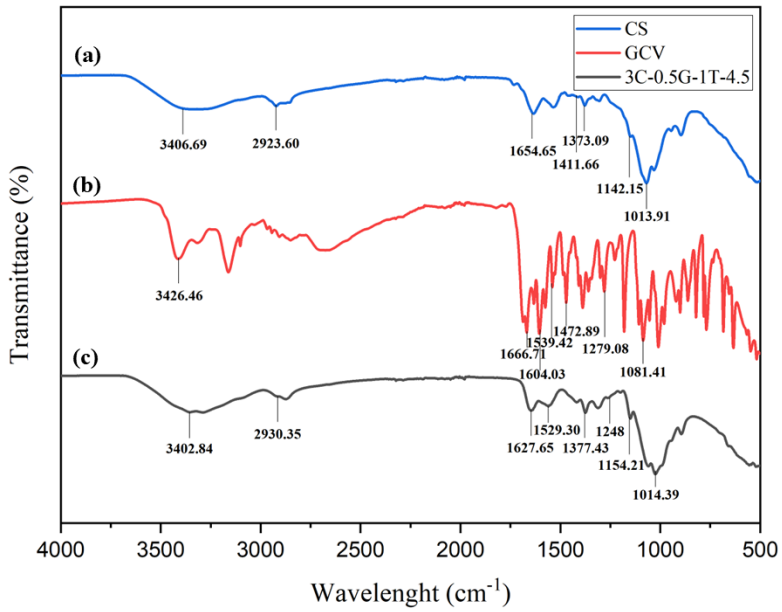

Figure 2. FT-IR Spectra of (a) CS, (b) GCV, and (c) 3C-0.5G-1T-4.5

The FTIR spectrum of CS in **Figure 2(a)** exhibits the identity bands at 1013.91 and 1142.15 cm^{-1}. They corresponded to the glycosidic linkage and the symmetrical bending of a glycosidic ring of CS, respectively. The bands at 1373.09 and 1411.66 cm^{-1} indicated the appearance of the remaining methyl groups (CH_3) in CS [56]. The specific band of the amine moieties in CS was found at 1654.65 cm^{-1} [57]. Meanwhile, the transmittance band at 2923.60 and 3406.69 cm^{-1} attributed to CH symmetric stretching and OH stretching, respectively [28].

DOI: https://doi.org/10.17509/ijost.v10i1.80998
p- ISSN 2528-1410 e- ISSN 2527-8045

The FTIR spectrum of GCV in **Figure 2(b)** shows the specific bands of C-O-C symmetric stretching at wavenumbers of 1081.41 and 1279.08 cm^{-1}. Moreover, the bands at 1472.89 and 1539.42 cm^{-1} attributed to aliphatic C–H bending, and C=N stretching, respectively. The bands at 1604.03 and 1666.71 cm^{-1} responded to the aromatic C=C in GCV molecules. The band at a wavenumber of 3426.46 cm^{-1} represented the N-H stretching [55,58].

The FTIR spectrum of 3C-0.5G-1T-4.5 is shown in **Figure 2(c).** It exhibits some identity bands of CS at various wavenumbers. 1014.39 and 1154.21 cm^{-1} corresponded to the glycosidic linkage and symmetrical bending of the glycosidic ring. The bands at 1377.43, 2930.35, and 3402.84 cm^{-1} represented the methyl groups, C-H stretching, and the hydroxyl group stretching in CS, respectively.

Furthermore, some specific bands of GCV molecules are found in this FTIR spectrum at 1529.30 and 1627.65 cm^{-1} which were consistent with the C=N stretching and aromatic C=C, respectively. These findings confirmed the entrapment of GCV in 3C-0.5G-1T-4.5. A band at a wavenumber of 1248 cm^{-1} represented the stretching vibration of P=O of the TPP molecules, which was a crosslinking agent in 3C-0.5G-1T-4.5 [29]. It evidenced the crosslink between the phosphate- and amine groups in TPP and CS, respectively, via electrostatic interactions.

Notably, the FTIR spectrum of 3C-0.5G-1T-4.5 exhibits clear shifts in the characteristic bands of CS and GCV, further confirming strong molecular interactions. The shifts in C=N and aromatic C=C bands of GCV, along with changes in the amine and phosphate-related bands of CS and TPP, highlight the electrostatic interactions stabilizing the nanoparticle system [59]. These spectral changes provide strong evidence of molecular interaction between GCV, CS, and TPP, contributing to the structural integrity of the formulated nanoparticles.

3.4. Results of release studies of GCV from GCV-CS-NPs

An *in vitro* drug release of GCV-CS-NPs was performed using modified Franz diffusion cells to investigate the release kinetic of GCV from 3C-0.5G-1T-4.5 as a representative of GCV-CS-NPs. In this study, 3C-0.5G-1T-4.5 was separated from the production medium pH 4.5 after the completion of the production process using the ultrafiltration technique. The obtained GCV-CS-NPs of 3C-0.5G-1T-4.5 were then reconstituted with PBS (pH 7.4), which is a pH of the vitreous humor, to obtain 0.1% w/v of GCV equivalent concentration before the release study.

3.4.1. Release of GCV from GCV-CS-NPs in PBS (pH 7.4)

The release profile of GCV from 3C-0.5G-1T-4.5 illustrated in **Figure 3** indicated the burst release of GCV in the first h of the study. Thereafter, the zero-order release kinetic of GCV from 3C-0.5G-1T-4.5 was found with an r^2 of 0.9824 in 7 h later.

This biphasic release kinetic of GCV from 3C-0.5G-1T-4.5 in PBS (pH 7.4) implied that in the initial study, GCV molecules, which were located on the surface of 3C-0.5G-1T-4.5, were immediately dissolved in the reconstituting medium. Therefore, 3C-0.5G-1T-4.5 already contained free GCV molecules in the vehicle that could quickly diffuse to the receiving medium following the concentration gradient of GCV [42]. GCV was gradually released from 3C-0.5G-1T-4.5 with a constant rate of 0.24±0.03 µg/min obeying the zero-order release kinetics.

Since this study was conducted using PBS (pH 7.4), it did not promote the dissolution of GCV and the swelling of the CS matrix because the pH of 7.4 was higher than the pKa values of GCV (pKa1), and CS, which were 2.2 and 6.5, respectively. Therefore, 3C-0.5G-1T-4.5 displayed as a reservoir of GCV and slowly released GCV molecules to the vehicle in according to the zero-order model [28].

DOI: https://doi.org/10.17509/ijost.v10i1.80998
p- ISSN 2528-1410 e- ISSN 2527-8045

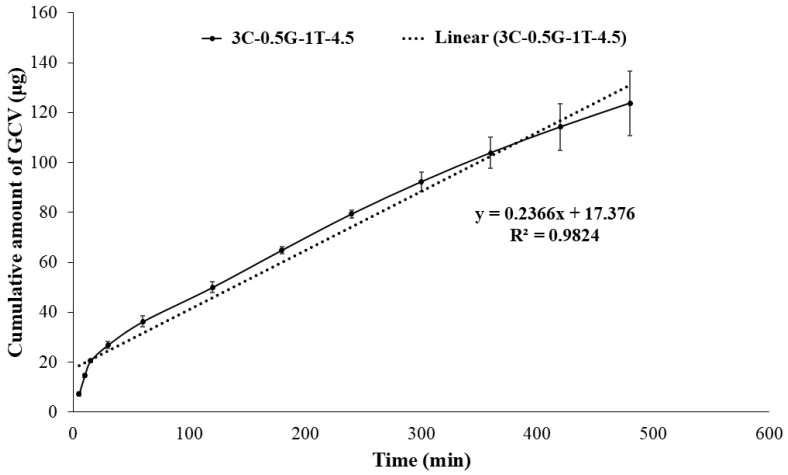

Figure 3. Drug release profiles of GCV from reconstituted 3C-0.5G-1T-4.5 (mean ± SD; n=3).

3.4.2. Diffusion of GCV from GCV-CS-NPs in the SVH

Since 3C-0.5G-1T-4.5 was aimed to inject into the vitreous humor, this study was conducted to mimic the application condition of GCV IVT injection by mixing each test sample, i.e., 3C-0.5G-1T-4.5 and GCV solution with the SVH, before determining the content of GCV in the receiving medium, which represented the intracellular biological fluid of the retinal cells, using Franz diffusion cells.

The diffusion profiles of GCV from 3C-0.5G-1T-4.5 and GCV solution are illustrated **in Figures 4(a) and 4(b)**. The diffusion profile shown in Fig. 4 (a1) indicated that the diffusion of GCV from 3C-0.5G-1T-4.5 through the SVH slowly occurred. This finding was due to not only the impediment of GCV movement by the CS matrix of 3C-0.5G-1T-4.5 and the matrix compositions of the SVH but also the pH of 7.4 of the SVH. As early discussed, this pH did not facilitate the release of GCV from 3C-0.5G-1T-4.5 because it did not promote the ionization of both GCV molecules and polymeric chains of CS in the NPs. Therefore, the release of GCV from 3C-0.5G-1T-4.5 affected the diffusion rate of GCV and led to slow diffusion of GCV in the SVH.

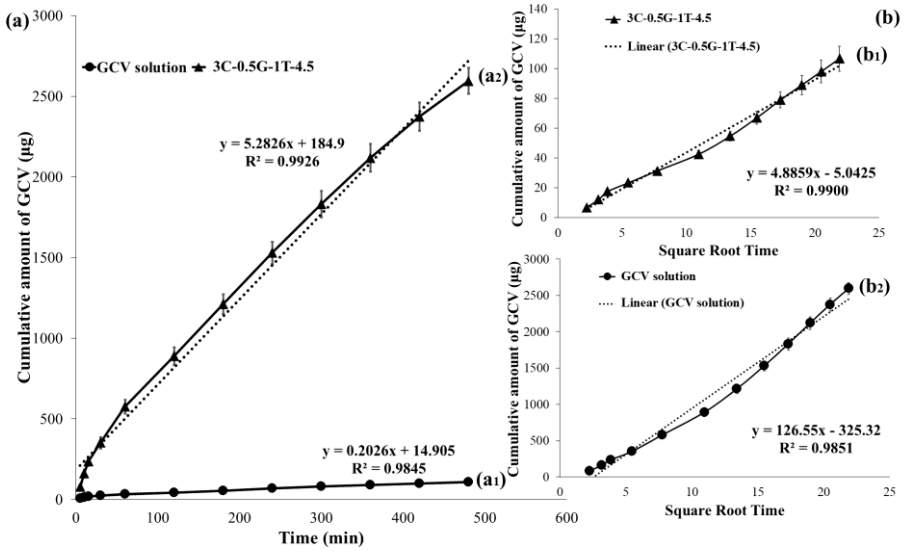

Figure 4. Diffusion profiles of GCV: (a) GCV diffusion through the SVH from 3C-0.5G-1T-4.5 (a1) and GCV solution (a2); and (b) the Higuchi's plots of GCV from 3C-0.5G-1T-4.5 (b1) and GCV solution (b2) (mean ± SD; n=3).

DOI: https://doi.org/10.17509/ijost.v10i1.80998
p- ISSN 2528-1410 e- ISSN 2527-8045

On the contrary, the diffusion of GCV from the GCV solution in the SVH was faster than that of GCV from 3C-0.5G-1T-4.5. In particular, in the first hour of the study, the sharp slope of the diffusion profile of the GCV solution was found. The GCV molecules could move through the SVH without impediment by the NPs matrix. Therefore, the GCV molecules were ready to diffuse by the concentration gradient of GCV. These results were consistent with the previous report by Weng *et al.* [60], in which the diffusion rate of drug molecules from PEGylated polymeric NPs was less than that of their molecules from the drug solution.

To determine the diffusion rate of GCV from 3C-0.5G-1T-4.5 and GCV solution in SVH, the cumulative amounts of GCV in the receiving medium were plotted against the square root of time by the criteria of Higuchi's release kinetic model and shown in **Figure 4(b)**. The diffusion of GCV from 3C-0.5G-1T-4.5 and GCV solution through the SVH obeyed Higuchi's model with an r^2 of 0.9900 and 0.9851, respectively. The diffusion rate of GCV from these dosage forms was 4.89±0.43 and 126.55±3.68 µg/min$^{1/2}$, respectively. The diffusion of GCV from 3C-0.5G-1T-4.5 was slower than GCV from GCV solution (*p*-value = 0.000) due to the controlled release of GCV by 3C-0.5G-1T-4.5 and the impediment of the SVH matrix. Since the diffusion of GCV was dominantly controlled by the SVH matrix, the biphasic drug release of GCV from 3C-0.5G-1T-4.5 could not be found in **Figure 4**.

3.5. Determination of an anti-HSV-1 activity of GCV-CS-NPs

This study was performed to determine the anti-HSV-1 activity of 3C-0.5G-1T-4.5 in the ARPE-19 cells, which were representative retinal cells and were the target cells for the treatment of herpetic retinitis using GCV IVT injection. Its activity was also compared to that of GCV solution and Blank-3C-1T-4.5.

3.5.1. Cell viability of the ARPE-19 cells incubated with the test samples

To determine the cytotoxicity of GCV solution, 3C-0.5G-1T-4.5 and Blank-3C-1T-4.5 to the ARPE-19 cells, the cells were incubated with the test samples at various equivalent concentrations of GCV in a range of 0.05-100 µg/mL for 24 h. Then, the cell viability of the ARPE-19 cells was determined by the MTT assay. The obtained results are illustrated in **Figure 5.**

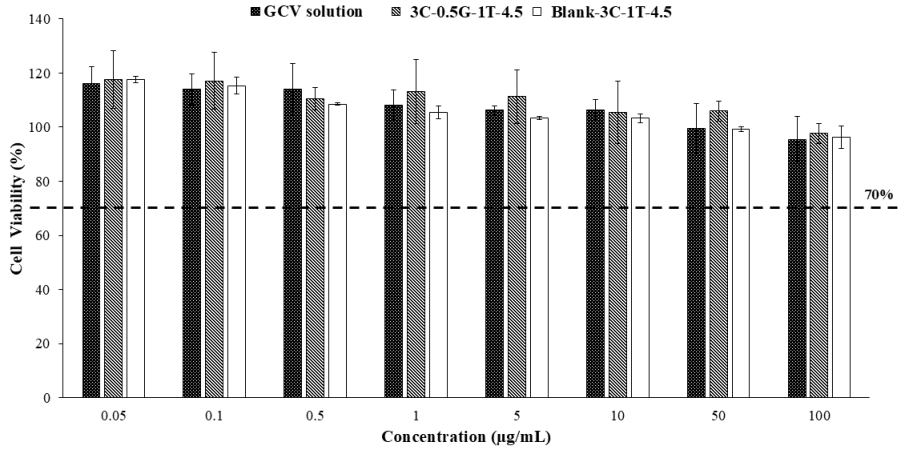

Figure 5. Viability of the ARPE-19 cells incubated with the test samples at various equivalent concentrations (mean ± SD; n=3).

The results shown in **Figure 5** evidenced that all equivalent concentrations of GCV solution, 3C-0.5G-1T-4.5 and Blank-3C-1T-4.5 used in this study were not toxic to the ARPE-19 cells. They provided around 100% viability of the ARPE-19 cells. All tested samples at the particular

DOI: https://doi.org/10.17509/ijost.v10i1.80998
p- ISSN 2528-1410 e- ISSN 2527-8045

range of equivalent concentrations were safe for the ARPE-19 cells. Therefore, the entire equivalent concentrations of GCV were used for determining an IC_{50} of each test sample against the HSV-1.

3.5.2. Results of the plaque assay

The plaque assay, which is one of the accurate methods for the direct quantification of infectious viruses by counting discrete plaques in cell culture [61], was performed to investigate the potential of GCV solution, 3C-0.5G-1T-4.5, and Blank-3C-1T-4.5 CS-NP for inhibiting the replication of the HSV-1 particles in the ARPE-19 cells.

Figure 6 shows that the higher the equivalent concentrations of GCV solution and 3C-0.5G-1T-4.5 have correlations to the lower the virus titer of the HSV-1 in the ARPE-19 cells. However, the anti-HSV-1 activity of Blank-3C-1T-4.5 was not found although its concentration was increased up to 100 µg/mL. The activity of GCV solution and 3C-0.5G-1T-4.5 against the HSV-1 was from the inhibitory activity of GCV by inhibiting the function of the viral deoxyribonucleic acid polymerase [3]. In this study, the IC_{50} which represents the ability of the test samples to inhibit 50% of the HSV-1 replication was also calculated. The IC_{50} of GCV solution and 3C-0.5G-1T-4.5 were 0.36±0.09 µg/mL and 25.12±0.02 µg/mL, respectively. The activity of the GCV solution against the HSV-1 was stronger than that of 3C-0.5G-1T-4.5. This finding was due to the controlled release of GCV from 3C-0.5G-1T-4.5. Therefore, GCV was slowly released from the NPs. It thus caused the delayed and weaker activity against the HSV-1 when compared to that of GCV from the GCV solution, which was prompt to exhibit its activity against the HSV-1.

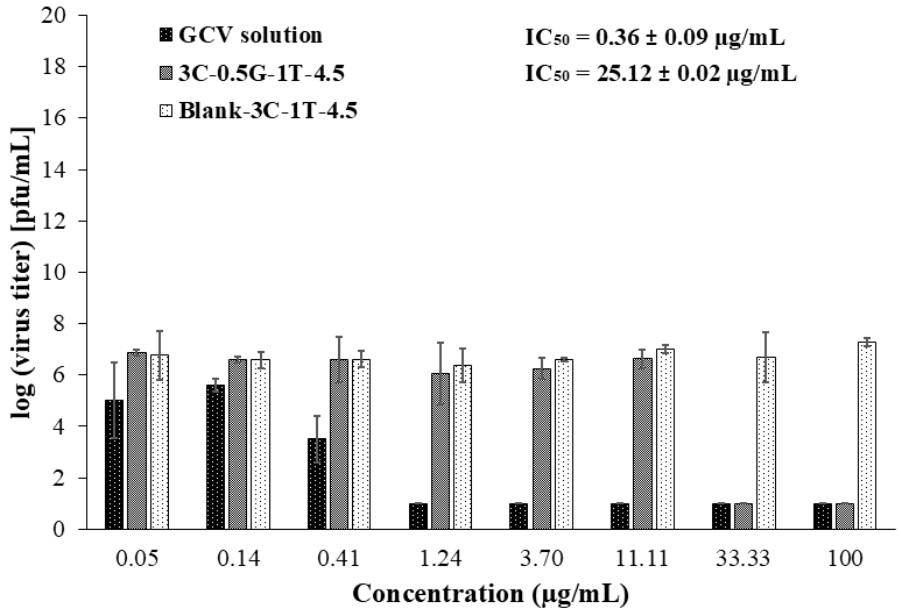

Figure 6. Viral titers of the HSV-1 in the ARPE-19 cells after incubation with the test samples for 24 h (mean ± SD; n=3).

This finding was consistent with the previous study reported by Kajiwara *et al.* [62]. The IC_{50} of GCV from PEGylated liposomes against HSV-1 was higher than that of GCV from GCV solution, due to the controlled release of the entrapped GCV in the liposomes.

Although 3C-0.5G-1T-4.5 could inhibit the replication of the HSV-1 particles with higher IC_{50} than that of GCV solution, the IC_{50} of 25.12±0.02 µg/mL was acceptable. Furthermore, 3C-0.5G-1T-4.5 provided some benefits for GCV IVT injection via the controlled release of the

DOI: https://doi.org/10.17509/ijost.v10i1.80998
p- ISSN 2528-1410 e- ISSN 2527-8045

GCV molecules leading to prolonged action of GCV and minimized frequency of the injections [23,24,26]. Therefore, 3C-0.5G-1T-4.5 could be accepted as a potential delivery system of GCV for the treatment of herpetic retinitis and could be subjected to further *in vivo* studies in appropriate animal models.

4. CONCLUSION

GCV-CS-NPs were successfully prepared in this study using the ionic gelation method. The formulations of GCV-CS-NPs were optimized by varying the content of CS, and GCV, including pH values of the production medium. All GCV-CS-NPs prepared in this study had a particle size in a nanometer range with moderate to high distribution. They had low to moderate positive zeta potential values depending on the formulation compositions. More importantly, their physicochemical properties were affected by the content of CS, GCV, and pH values of the production medium. The optimized GCV-CS-NPs obtained in this study were 3C-0.5G-1T-4.5. It was prepared at a pH of 4.5 and contained CS/GCV/TPP at a weight ratio of 3/0.5/1, respectively. The obtained 3C-0.5G-1T-4.5 could control the release of GCV by the zero-order release kinetic model. GCV molecules from 3C-0.5G-1T-4.5 diffused through the SVH in agreement with Higuchi's model. The obtained 3C-0.5G-1T-4.5 had an anti-HSV-1 activity with an IC50 of 25.12±0.02 µg/mL. Therefore, 3C-0.5G-1T-4.5 could be accepted as a potential delivery system of GCV to the vitreous humor via IVT injection. Furthermore, it could be subjected to further in vivo studies in the appropriate animal models to investigate its anti-HSV-1 efficacy and its safety for IVT injection.

5. ACKNOWLEDGMENT

The authors gratefully acknowledged the financial support by 1) Specialized Research Grants Faculty of Pharmacy, Thammasat University (Contract No. Pharm TU-S-D 1/2024), 2) Thammasat University Research Unit in Drug, Health Product Development and Application (DHP-DA (Project ID. 6305001), 3) the National Research Council of Thailand (NRCT) and Thamassat University for Mid-Career Research (Grant No. N42A650328).

6. AUTHORS' NOTE

The authors declare that there is no conflict of interest regarding the publication of this article. The authors confirmed that the paper was free of plagiarism.

7. REFERENCES

[1] Bagga, B., Kate, A., Joseph, J., and Dave, V. P. (2020). Herpes simplex infection of the eye: an introduction. *Community Eye Health*, *33*(108), 68–70.

[2] McCormick, I., James, C., Welton, N. J., Mayaud, P., Turner, K. M. E., Gottlieb, S. L., Foster, A., and Looker, K. J. (2022). Incidence of herpes simplex virus keratitis and other ocular disease: Global review and estimates. *Ophthalmic Epidemiology*, *29*(4), 353–362.

[3] Choudhari, M., Nayak, K., Nagai, N., Nakazawa, Y., Khunt, D., and Misra, M. (2023). Role of mucoadhesive agent in ocular delivery of ganciclovir microemulsion: Cytotoxicity evaluation in vitro and ex vivo. *International Ophthalmology*, *43*(4), 1153–1167.

[4] Heikkinen, E. M., Ruponen, M., Jasper, L. M., Leppanen, J., Hellinen, L., Urtti, A., and Vellonen, K. S. (2020). Prodrug approach for posterior eye drug delivery: synthesis of

novel ganciclovir prodrugs and in vitro screening with cassette dosing. *Molecular Pharmaceutics*, *17*(6), 1945-1953.

[5] Yu, T., Peng, R. M., Xiao, G. G., Feng, L. N., and Hong, J. (2020). Clinical evaluation of intravitreal injection of ganciclovir in refractory corneal endotheliitis. *Ocular Immunology and Inflammation*, *28*(2), 270-280.

[6] Verrecchia, S., El Chehab, H., Chudzinski, R., Chaperon, M., Levron, A., Agard, E., and Dot, C. (2019). Does repeated intravitreal injections impact the quality of life of patients, about 40 patients? *Investigative Ophthalmology & Visual Science*, *60*(9), 4471-4471.

[7] Wang, Q., Sun, C., Xu, B., Tu, J., and Shen, Y. (2018). Synthesis, physicochemical properties and ocular pharmacokinetics of thermosensitive in situ hydrogels for ganciclovir in cytomegalovirus retinitis treatment. *Drug Delivery*, *25*(1), 59-69.

[8] Sims, L., Ramasubramanian, A., and Steinbach-Rankins, J. M. (2018). Novel PLGA nanoparticles encapsulating melphalan for the treatment of retinoblastomas. *Investigative Ophthalmology & Visual Science*, *59*(9), 4963-4963.

[9] Varshochian, R., Riazi-Esfahani, M., Jeddi-Tehrani, M., Mahmoudi, A. R., Aghazadeh, S., Mahbod, M., and Dinarvand, R. (2015). Albuminated PLGA nanoparticles containing bevacizumab intended for ocular neovascularization treatment. *Journal of Biomedical Materials Research Part A*, *103*(10), 3148-3156.

[10] Canioni, R., Reynaud, F., Leite-Nascimento, T., Gueutin, C., Guiblin, N., Ghermani, N. E., and Tsapis, N. (2021). Tiny dexamethasone palmitate nanoparticles for intravitreal injection: Optimization and in vivo evaluation. *International Journal of Pharmaceutics*, *600*, 120509.

[11] Yang, C., Yang, J., Lu, A., Gong, J., Yang, Y., Lin, X., and Xu, H. (2022). Nanoparticles in ocular applications and their potential toxicity. *Frontiers in Molecular Biosciences*, *9*, 931759.

[12] Swetledge, S., Jung, J. P., Carter, R., and Sabliov, C. (2021). Distribution of polymeric nanoparticles in the eye: implications in ocular disease therapy. *Journal of Nanobiotechnology*, *19*(1), 10.

[13] Beach, M. A., Nayanathara, U., Gao, Y., Zhang, C., Xiong, Y., Wang, Y., and Such, G. K. (2024). Polymeric nanoparticles for drug delivery. *Chemical Reviews*, *124*(9), 5505-5616.

[14] Zielińska, A., Carreiró, F., Oliveira, A. M., Neves, A., Pires, B., Venkatesh, D. N., Durazzo, A., Lucarini, M., Eder, P., Silva, A. M., Santini, A., and Souto, E. B. (2020). Polymeric nanoparticles: Production, characterization, toxicology and ecotoxicology. *Molecules (Basel, Switzerland)*, *25*(16), 3731.

[15] Weißpflog, J., Vehlow, D., Müller, M., Kohn, B., Scheler, U., Boye, S., and Schwarz, S. (2021). Characterization of chitosan with different degree of deacetylation and equal viscosity in dissolved and solid state–Insights by various complimentary methods. *International Journal of Biological Macromolecules*, *171*, 242-261.

[16] Popova, E. V., Tikhomirova, V. E., Beznos, O. V., Chesnokova, N. B., Grigoriev, Y. V., and Kost, O. A. (2023). Chitosan Nanoparticles: The drug delivery system to the anterior segment of the eye. *Moscow University Chemistry Bulletin*, *78*(2), 82-88.

DOI: https://doi.org/10.17509/ijost.v10i1.80998
p- ISSN 2528-1410 e- ISSN 2527-8045

[17] Burhan, A. M., Klahan, B., Cummins, W., Andrés-Guerrero, V., Byrne, M. E., O'Reilly, N. J., Chauhan, A., Fitzhenry, L., and Hughes, H. (2021). Posterior segment ophthalmic drug delivery: Role of muco-adhesion with a special focus on chitosan. *Pharmaceutics*, *13*(10), 1685.

[18] Goyal, S., Thirumal, D., Rana, J., Gupta, A. K., Kumar, A., Babu, M. A., and Sindhu, R. K. (2024). Chitosan based nanocarriers as a promising tool in treatment and management of inflammatory diseases. *Carbohydrate Polymer Technologies and Applications*, *7*, 100442.

[19] Lozano Chamizo, L., Luengo Morato, Y., Ovejero Paredes, K., Contreras Caceres, R., Filice, M., and Marciello, M. (2021). ionotropic gelation-based synthesis of chitosan-metal hybrid nanoparticles showing combined antimicrobial and tissue regenerative activities. *Polymers*, *13*(22), 3910.

[20] Asasutjarit, R., Sorrachaitawatwong, C., Tipchuwong, N., and Pouthai, S. (2013). Effect of formulation compositions on particle size and zeta potential of diclofenac sodium-loaded chitosan nanoparticles. *International Journal of Pharmacological and Pharmaceutical Sciences*, *7*(9), 568-570.

[21] Patel, R., Gajra, B., Parikh, R. H., and Patel, G. (2016). Ganciclovir loaded chitosan nanoparticles: preparation and characterization. *Journal Nanomedicine Nanotechnology*, *7*(6), 1-8.

[22] Albarqi, H. A., Garg, A., Ahmad, M. Z., Alqahtani, A. A., Walbi, I. A., and Ahmad, J. (2023). Recent progress in chitosan-based nanomedicine for its ocular application in glaucoma. *Pharmaceutics*, *15*(2), 681.

[23] Mikušová, V., and Mikuš, P. (2021). Advances in chitosan-based nanoparticles for drug delivery. *International Journal of Molecular Sciences*, *22*(17), 9652.

[24] Lu, Y., Zhou, N., Huang, X., Cheng, J. W., Li, F. Q., Wei, R. L., and Cai, J. P. (2014). Effect of intravitreal injection of bevacizumab-chitosan nanoparticles on retina of diabetic rats. *International Journal of Ophthalmology*, *7*(1), 1–7.

[25] Alkholief, M., Kalam, M. A., Raish, M., Ansari, M. A., Alsaleh, N. B., Almomen, A., Ali, R., and Alshamsan, A. (2023). Topical sustained-release dexamethasone-loaded chitosan nanoparticles: Assessment of drug delivery efficiency in a rabbit model of endotoxin-induced uveitis. *Pharmaceutics*, *15*(9), 2273.

[26] Elsaid, N., Jackson, T. L., Elsaid, Z., Alqathama, A., and Somavarapu, S. (2016). PLGA microparticles entrapping chitosan-based nanoparticles for the ocular delivery of ranibizumab. *Molecular Pharmaceutics*, *13*(9), 2923-2940.

[27] Asasutjarit, R., Managit, C., Phanaksri, T., Treesuppharat, W., and Fuongfuchat, A. (2020). Formulation development and in vitro evaluation of transferrin-conjugated liposomes as a carrier of ganciclovir targeting the retina. *International Journal of Pharmaceutics*, *577*, 119084.

[28] Ullah, S., Azad, A. K., Nawaz, A., Shah, K. U., Iqbal, M., Albadrani, G. M., and Abdel-Daim, M. M. (2022). 5-fluorouracil-loaded folic-acid-fabricated chitosan nanoparticles for site-targeted drug delivery cargo. *Polymers*, *14*(10), 2010.

DOI: https://doi.org/10.17509/ijost.v10i1.80998
p- ISSN 2528-1410 e- ISSN 2527-8045

[29] Asasutjarit, R., Theerachayanan, T., Kewsuwan, P., Veeranodha, S., Fuongfuchat, A., and Ritthidej, G. C. (2015). Development and evaluation of diclofenac sodium loaded-N-trimethyl chitosan nanoparticles for ophthalmic use. *AAPS Pharmscitech*, *16*, 1013-1024.

[30] Purnama, L. M. J., Witchitchan, R., Fristiohady, A., Uttarawichien, T., Payuhakrit, W., and Asasutjarit, R. (2024). Formulation development of thermoresponsive quercetin nanoemulgels and in vitro investigation of their inhibitory activity on vascular endothelial growth factor-A inducing neovascularization from the retinal pigment epithelial cells. *Journal of Drug Delivery Science and Technology*, *100*(6), 106005.

[31] Schulz, A., and Szurman, P. (2022). Vitreous substitutes as drug release systems. *Translational Vision Science & Technology*, *11*(9), 14.

[32] Bonfiglio, A., Lagazzo, A., Repetto, R., and Stocchino, A. (2015). An experimental model of vitreous motion induced by eye rotations. *Eye and Vision*, *2*, 10.

[33] Yin, Y., Li, J., Su, L., Ou, Z., Lv, Q., Xiao, M., Wang, C., Zeng, D., Gu, Y., Yang, F., Chen, M., Feng, S., Hu, W., Bu, F., Zhu, B., and Xu, Y. (2023). Screening and verification of antiviral compounds against HSV-1 using a method based on a plaque inhibition assay. *BMC Infectious Diseases*, *23*(1), 890.

[34] Thongchai, S., Ekalaksananan, T., Pientong, C., Aromdee, C., Seubsasana, S., Sukpol, C., and Kongyingyoes, B. (2008). Anti-herpes simplex virus type 1 activity of crude ethyl acetate extract derived from leaves of Clinacanthus nutans Lindau. *KKU Research Journal (Graduate Studies)*, *8* (2), 65-73.

[35] Rodrigues, S., da Costa, A. M., and Grenha, A. (2012). Chitosan/carrageenan nanoparticles: effect of cross-linking with tripolyphosphate and charge ratios. *Carbohydrate Polymers*, *89*(1), 282–289.

[36] Thomas, O. E., and Adegoke, O. A. (2015). Development of a visible spectrophotometric method for the analysis of ganciclovir in bulk sample and dosage form. *Tropical Journal of Pharmaceutical Research*, *14*(6), 1095-1101.

[37] Zaman, P., Wang, J., Blau, A., Wang, W., Li, T., Kohane, D. S., Loscalzo, J., and Zhang, Y. Y. (2016). Incorporation of heparin-binding proteins into preformed dextran sulfate-chitosan nanoparticles. *International Journal of Nanomedicine*, *11*, 6149–6159.

[38] Jintapattanakit, A., Junyaprasert, V. B., Mao, S., Sitterberg, J., Bakowsky, U., and Kissel, T. (2007). Peroral delivery of insulin using chitosan derivatives: a comparative study of polyelectrolyte nanocomplexes and nanoparticles. *International Journal of Pharmaceutics*, *342*(1-2), 240–249.

[39] Danial, S., Gamal, F., Saad, N., Hamdy, H., Adel, G., Elnahas, M., and Wagdy, H. A. (2023). Simple Green RP-UPLC. Method for the analysis of ganciclovir in its bulk form and pharmaceutical preparations. *Egyptian Journal of Chemistry*, *66*(9), 133-143.

[40] Lim, C., Shin, Y., and Oh, K. T. (2024). Polyelectrolyte complex for drug delivery. *Drug Targets and Therapeutics*, *3*(1), 62-73.

[41] Hussain, Z, and Sahudin, S. (2016). Preparation, characterisation and colloidal stability of chitosan-tripolyphosphate nanoparticles: Optimisation of formulation and process

DOI: https://doi.org/10.17509/ijost.v10i1.80998
p- ISSN 2528-1410 e- ISSN 2527-8045

parameters. *International Journal of Pharmacy and Pharmaceutical Science*, *8*(3), 297-308.

[42] Herdiana, Y., Wathoni, N., Shamsuddin, S., and Muchtaridi, M. (2021). Drug release study of the chitosan-based nanoparticles. *Heliyon*, *8*(1), e08674.

[43] Moraru, C., Mincea, M., Menghiu, G., and Ostafe, V. (2020). Understanding the factors influencing chitosan-based nanoparticles-protein corona interaction and drug delivery applications. *Molecules*, *25*(20), 4758.

[44] Katas, H., Raja, M. A., and Lam, K. L. (2013). Development of chitosan nanoparticles as a stable drug delivery system for protein/siRNA. *International Journal of Biomaterials*, 2013, 146320.

[45] Pagar, K., and Vavia, P. (2013). Rivastigmine-loaded L-lactide-depsipeptide polymeric nanoparticles: decisive formulation variable optimization. *Scientia Pharmaceutica*, *81*(3), 865–885.

[46] Aranaz, I., Alcántara, A. R., Civera, M. C., Arias, C., Elorza, B., Heras Caballero, A., and Acosta, N. (2021). Chitosan: An overview of its properties and applications. *Polymers*, *13*(19), 3256.

[47] Wang, L., Zhou, M. B., and Zhang, H. (2021). The emerging role of topical ocular drugs to target the posterior eye. *Ophthalmology and Therapy*, *10*(3), 465–494.

[48] Sobolewska, B., Heiduschka, P., Bartz-Schmidt, K. U., and Ziemssen, F. (2017). pH of anti-VEGF agents in the human vitreous: low impact of very different formulations. *International Journal of Retina and Vitreous*, *3*, 22.

[49] Gontijo, L. A. P., Raphael, E., Ferrari, D. P. S., Ferrari, J. L., Lyon, J. P., and Schiavon, M. A. (2020). pH effect on the synthesis of different size silver nanoparticles evaluated by DLS and their size-dependent antimicrobial activity. *Matéria*, *25*(04), e-12845.

[50] Clayton, K. N., Salameh, J. W., Wereley, S. T., and Kinzer-Ursem, T. L. (2016). Physical characterization of nanoparticle size and surface modification using particle scattering diffusometry. *Biomicrofluidics*, *10*(5), 054107.

[51] Pilipenko, I., Korzhikov-Vlakh, V., Sharoyko, V., Zhang, N., Schäfer-Korting, M., Rühl, E., Zoschke, C., and Tennikova, T. (2019). pH-sensitive chitosan-heparin nanoparticles for effective delivery of genetic drugs into epithelial cells. *Pharmaceutics*, *11*(7), 317.

[52] Nallamuthu, I., Devi, A., and Khanum, F. (2015). Chlorogenic acid loaded chitosan nanoparticles with sustained release property, retained antioxidant activity and enhanced bioavailability. *Asian Journal of Pharmaceutical Sciences*, *10*(3), 203-211.

[53] Chanphai, P., Konka, V., and Tajmir-Riahi, H. A. (2017). Folic acid–chitosan conjugation: A new drug delivery tool. *Journal of Molecular Liquids*, *238*, 155-159.

[54] Yang, S. J., Lin, F. H., Tsai, K. C., Wei, M. F., Tsai, H. M., Wong, J. M., and Shieh, M. J. (2010). Folic acid-conjugated chitosan nanoparticles enhanced protoporphyrin IX accumulation in colorectal cancer cells. *Bioconjugate Chemistry*, *21*(4), 679-689.

[55] Gaber, D. A., Alnwiser, M. A., Alotaibi, N. L., Almutairi, R. A., Alsaeed, S. S., Abdoun, S. A., and Alsubaiyel, A. M. (2022). Design and optimization of ganciclovir solid dispersion for improving its bioavailability. *Drug Delivery*, *29*(1), 1836-1847.

DOI: https://doi.org/10.17509/ijost.v10i1.80998
p- ISSN 2528-1410 e- ISSN 2527-8045

[56] Gatta, A. K., Chandrashekhar, R., Udupa, N., Reddy, M. S., Mutalik, S., and Josyula, V. R. (2020). Strategic design of dicer substrate siRNA to mitigate the resistance mediated by ABCC1 in doxorubicin-resistant breast cancer. *Indian Journal of Pharmaceutical Sciences*, *82*(2), 329-340.

[57] Ayodele, O., Okoronkwo, A. E., Oluwasina, O. O., and Abe, T. O. (2018). Utilization of blue crab shells for the synthesis of chitosan nanoparticles and their characterization. *Songklanakarin Journal of Science and Technology*, *40*, 1039-1042.

[58] Mishra, A., Sinha, V. R., Sharma, S., Mathew, A. T., Kumar, R., and Yadav, A. K. (2023). A comprehensive compatibility study of ganciclovir with some common excipients. *American Journal of Biopharmacy and Pharmaceutical Sciences*, *3*(2), 1-10.

[59] Sawdon, A. J., Zhang, J., Peng, S., Alyami, E. M., and Peng, C. A. (2021). Polymeric nanovectors incorporated with ganciclovir and HSV-*TK* encoding plasmid for gene-directed enzyme prodrug therapy. *Molecules*, *26*(6), 1759.

[60] Weng, J., Tong, H. H. Y., and Chow, S. F. (2020). In vitro release study of the polymeric drug nanoparticles: Development and validation of a novel method. Pharmaceutics, *12*(8), 732.

[61] Mendoza, E. J., Manguiat, K., Wood, H., and Drebot, M. (2020). Two detailed plaque assay protocols for the quantification of infectious SARS-CoV-2. *Current Protocols in Microbiology*, *57*(1), cpmc105.

[62] Kajiwara, E., Kawano, K., Hattori, Y., Fukushima, M., Hayashi, K., and Maitani, Y. (2007). Long-circulating liposome-encapsulated ganciclovir enhances the efficacy of HSV-TK suicide gene therapy. *Journal of Controlled Release: Official Journal of the Controlled Release Society, 120*(1-2), 104–110.

DOI: https://doi.org/10.17509/ijost.v10i1.80998
p- ISSN 2528-1410 e- ISSN 2527-8045